communications earth & environment

Article

A Nature Portfolio journal

https://doi.org/10.1038/s43247-025-03067-6

Nutrient limitation regimes control sunlight-stimulated chlorophyll fluorescence in the South Atlantic Ocean

Tiera-Brandy Robinson [1] ✉, Haoran Liu[1,2], Shungudzemwoyo P. Garaba[3], Daniela Voss [3], Nina Schuback [4,5], C. Mark Moore[6], Kevin Oxborough[5], Eric P. Achterberg [1] & Thomas J. Browning [1]

Sunlight-stimulated chlorophyll fluorescence offers potential for assessing phytoplankton physiological status at broad scales detected by satellites, but controls on these signals are poorly constrained. In this study, we present a comprehensive, high-resolution dataset of passive chlorophyll fluorescence alongside potential physical and biogeochemical drivers collected across the Benguela upwelling system and South Atlantic Subtropical Gyre. The nutrient limitation status of phytoplankton was assessed through 27 onboard bioassay experiments. A consistent and significant difference in light-saturated, passive chlorophyll fluorescence normalized to phytoplankton absorption ($F/a_{ph}^{passive}_{max}$) was observed between waters where phytoplankton were either iron or nitrogen limited, with iron limited regions showing threefold higher $F/a_{ph}^{passive}_{max}$ compared to nitrogen limited regions. When interpreted alongside the results of the bioassay experiments, we found that neither variability in physical forcing (temperature, mixing, light climate) or phytoplankton community structure could explain the major variability in $F/a_{ph}^{passive}_{max}$. These results provide direct field-based evidence that passive chlorophyll fluorescence is sensitive to phytoplankton nutrient limitation and demonstrates potential for observation at high spatial and temporal resolution using satellite observations.

Chlorophyll (Chl) fluorescence refers to emission of red light from chlorophyll-a (Chl *a*) molecules following light absorption at shorter wavelengths and can be stimulated actively or passively (Table S1)[1]. Here we define active fluorometry as the stimulation of Chl fluorescence emission by high photon irradiance light pulses (typically 100 to 200 µs duration at >20,000 µmol photons m^{-2} s^{-1}) directed at (typically dark-acclimated) phytoplankton. In contrast, we define passive fluorescence as the stimulation of Chl fluorescence by sunlight. Both active and passive Chl fluorescence show a first order correlation with Chl *a* concentration, whilst also being strongly influenced by phytoplankton ecophysiology[1]. As a result, active or passive fluorescence normalized to Chl *a* concentrations shows large variability[2–7]. Therefore, the utilization of Chl fluorescence as an index of either Chl *a* concentrations or phytoplankton physiology requires an understanding of physiological, ecological, and environmental drivers.

As a result of the large difference in excitation sources (i.e., intensity, duration, spectral shape), active and passive Chl fluorescence signals are not equivalent and therefore may respond differently to a range of environmental and ecological drivers[1,8–10]. Excitation intensity and duration result in different forms of, and measurement positions along, fluorescence induction curves[1]. For example, as a result of differences in excitation intensity, diel cycles in active and passive chlorophyll fluorescence show a general inverse correlation[4,5], with no robust means to convert between them. As almost all direct assessments of the drivers of Chl fluorescence have come from active measurements e.g,[7,11], this presents a problem for the interpretation of passive fluorescence[4,5]. A reliable interpretation of passive fluorescence could provide invaluable information on phytoplankton physiology at global scales, as it can be detected by satellite remote sensing[10,12,13].

Observations of passive Chl fluorescence by sensors on satellites rely on the determination of the fluorescence line height from upwelled water-leaving radiance via subtraction of a baseline constructed from adjacent wavebands on either side of the peak[12,14]. Chl *a* concentrations can be determined independently from the ratio of radiances in blue and green portions of the spectrum and their empirical relationship with Chl *a*

[1]Marine Biogeochemistry Division, GEOMAR Helmholtz Centre for Ocean Research Kiel, Kiel, Germany. [2]State Key Laboratory of Marine Environmental Science, Xiamen University, Xiamen, Fujian, China. [3]Niedersächsische Zentrum für Marine Sensorik, Carl von Ossietzky Universität Oldenburg, Wilhelmshaven, Germany. [4]Swiss Polar Institute, Sion, Switzerland. [5]Chelsea Technologies Ltd., Yateley, UK. [6]School of Ocean and Earth Science, National Oceanography Centre Southampton, University of Southampton, Southampton, UK. ✉e-mail: brobinson@geomar.de

concentration[15]. Both remote sensing of passive Chl fluorescence and Chl *a* concentrations derived from blue: green radiance ratios can be undertaken by field radiometric measurements, therefore offering a potential means to thoroughly assess the controls on passive fluorescence[5,6].

Aside from light limited growth at higher latitudes in winter, experiments have demonstrated that phytoplankton growth across most of the ocean surface is generally limited by two nutrients, nitrogen (N) and/or iron (Fe)[16]. The response of active Chl fluorescence signals to these nutrient limitations has been investigated across a range of field and laboratory experiments[16–20]. Despite important variability and exceptions, a general observed trend is that under conditions of N limitation, active fluorescence per unit Chl is low, whereas under Fe limitation it is elevated[11,16,18,21]. Elevated Chl-normalized active fluorescence under Fe limitation is thought to be a result of (i) higher ratios of highly fluorescent photosystem II (PSII) to largely non-fluorescent photosystem I (PSI), due to the much higher Fe requirements for PSI in comparison to PSII and (ii) less efficient energetic coupling between some of the pigment-protein complexes present and functional PSII reaction centers[5,11,22].

Recent observations have shown that the effects of N versus Fe limitation on active Chl fluorescence may extend to observations of passive fluorescence[5]. Specifically, in the tropical Pacific, Chl-normalized light-saturated passive fluorescence was found to be elevated around threefold under Fe limited conditions in comparison to N limited conditions[5]. However, this study encountered minimal variability in upper ocean light climates, temperatures, phytoplankton concentrations and community structure[5], which could all potentially co-regulate passive Chl fluorescence signals alongside nutrient limitation at larger spatial-temporal scales in the ocean[10,13]. The widespread applicability of passive Chl-normalized fluorescence as an indicator of N versus Fe limitation therefore remains unexplored with direct field observations.

The Benguela upwelling region is among the most productive coastal upwelling zones globally and transitions into the low productivity waters of the South Atlantic Subtropical Gyre[23]. Collectively the region hosts major gradients in environmental conditions (including seawater temperatures, mixing of the upper water column, light climate, nutrient supply) and phytoplankton (Chl *a* concentrations, community structure), making it an ideal site for investigating the multiple potential drivers of passive Chl fluorescence[24]. Reduced sea surface temperatures alongside elevated nutrient concentrations as well as phytoplankton biomass in the Benguela are driven by coastal upwelling, which transitions offshore into the warmer, highly stratified and low nutrient waters of the South Atlantic Gyre[25]. Coastal upwelled waters in the Benguela system are transferred to the gyre in eddies and filaments (distinct, elongated features flowing offshore), transporting nutrients, phytoplankton, and other properties of the upwelled waters with them[26,27]. In this study, we tracked two filaments extending >400 km off the coast of Namibia before they dissipated, as well as undertaking a transect from the upwelling zone into the South Atlantic Subtropical Gyre. High spatial and temporal resolution passive fluorescence measurements were paired with a range of ancillary measurements of ocean physics and biogeochemistry made at the same sites. We find that the phytoplankton nutrient limitation regime controls most of the variability in absorption-normalized light-saturated passive fluorescence, supporting its widespread application to satellite remote sensing.

Methods

Study location and sampling

Sample collection, experiments, and radiometric measurements were conducted aboard RV Meteor during cruise M187 from 25th January to 4th March 2023. The cruise track covered the area in the Benguela upwelling region and South Atlantic Gyre (Fig. 1). Station sampling was conducted during the day from ca. 08:30–17:00 local time, with transits between stations in the evening/night time. Further underway samples were collected during transit between stations. Water column profiles of salinity and temperature as well as discrete water samples were collected for each station daily using a Sea-Bird conductivity-temperature-depth probe (CTD, SBE 911Plus, Sea-Bird Scientific) with water carousel. Surface water samples were collected whilst the ship was steaming using a customized towed water sampling device (so called 'tow-fish'), outfitted with acid-washed tubing and Teflon bellows pump (Dellmeco A15) and was deployed alongside the ship at 2–3 m depth. Tow-fish samples were pumped into a specialized trace-metal-clean air bubble, where positive air pressure was maintained by directing inward airflow through a high-efficiency particle air filter.

Mixed Layer Depth (MLD)

Mixed layer depth (*MLD*) was calculated using CTD profiles at each station. The *MLD* was defined using a temperature threshold criterion adapted from de Boyer Montégut, et al.[28]. Specifically, the reference depth was fixed at 12 m, and the *MLD* was identified as the shallowest depth where the temperature had decreased by more than 0.2 °C relative to the reference temperature.

Vertical Diffuse Attenuation Coefficient (K_d)

K_d was determined from downwelling irradiance measurements using the Sea-Bird Scientific free-falling HyperPro II profiling system. The profiling system is designed for slow vertical descent in-water optical measurements[29]. It has two hyperspectral HyperOCR radiometers ($\lambda = 350–800$ nm) integrated to measuring downwelling $E_D(\lambda)$ and upwelling $L_u(\lambda)$ irradiance. A third radiometer installed on the ship stern, measured above-water downwelling irradiance $E_D(\lambda)$ for normalization and cloud correction. Deployment of the profiler system was from the stern of the ship followed by monitored drift to at least 30 m away to avoid ship shadowing. At each station, 1–3 profile casts were recorded, extending to at least 1% light level assumed to be the euphotic zone depth. Profiles were recorded using SatView software (v2.9.5_7). During processing, data with instrument tilt >5° were discarded to ensure optimal vertical orientation. For each profile, a linear regression was applied to the natural logarithm of spectrally integrated downwelling irradiance versus depth:

$$ln\left(E_D(z)\right) = ln\left(E_0\right) - K_d \cdot z \quad (1)$$

K_d was derived as the negative slope of the regression. Photosynthetically active radiation (PAR) was calculated as spectrally-integrated values of $E_D(\lambda = 400 - 700\text{nm})$, and depth vs. ln (PAR) plots were generated with fitted regression lines for quality assurance. Where multiple profiles were available per station, K_d values were averaged.

Mixed layer irradiance ($\widetilde{E_g}$)

The median mixed layer irradiance ($\widetilde{E_g}$) was estimated by integrating the exponential decay of light from the surface to the *MLD*:

$$\widetilde{E_g} = \bar{E}_0 e^{-k_d * \left(\frac{MLD}{2}\right)} \quad (2)$$

Where $\bar{E}_0$ is the daily-mean surface irradiance (mol photons m^{-2} h^{-1}), K_d is the diffuse attenuation coefficient (m^{-1}), and *MLD* is the mixed layer depth (m). This equation assumes a homogeneous water column within the mixed layer and negligible internal sources of irradiance. $\widetilde{E_g}$ values were calculated for each station with available *MLD*, K_d, and $\bar{E}_0$ data.

Satellite observations

Standard Level 3, 4 km resolution, Chl and sea surface temperature (SST) products from Moderate Resolution Imaging Spectroradiometer (MODIS-Aqua) were retrieved from NASA Earthdata repository https://oceandata.sci.gsfc.nasa.gov/l3/ (reprocessing 2022 for Chl data and reprocessing 2019 for SST data). The download data matched the field survey with the aim to examine the spatial and temporal variability in the Benguela upwelling region and to monitor the progression and movement of the filaments and surrounding eddy systems. Additional 8-day average, 4 km resolution data was downloaded for standard Level 3 MODIS and provisional Plankton, Aerosol, Cloud, ocean Ecosystem (PACE) normalized fluorescence line height (nFLH) and Chl products for the study region during the time period

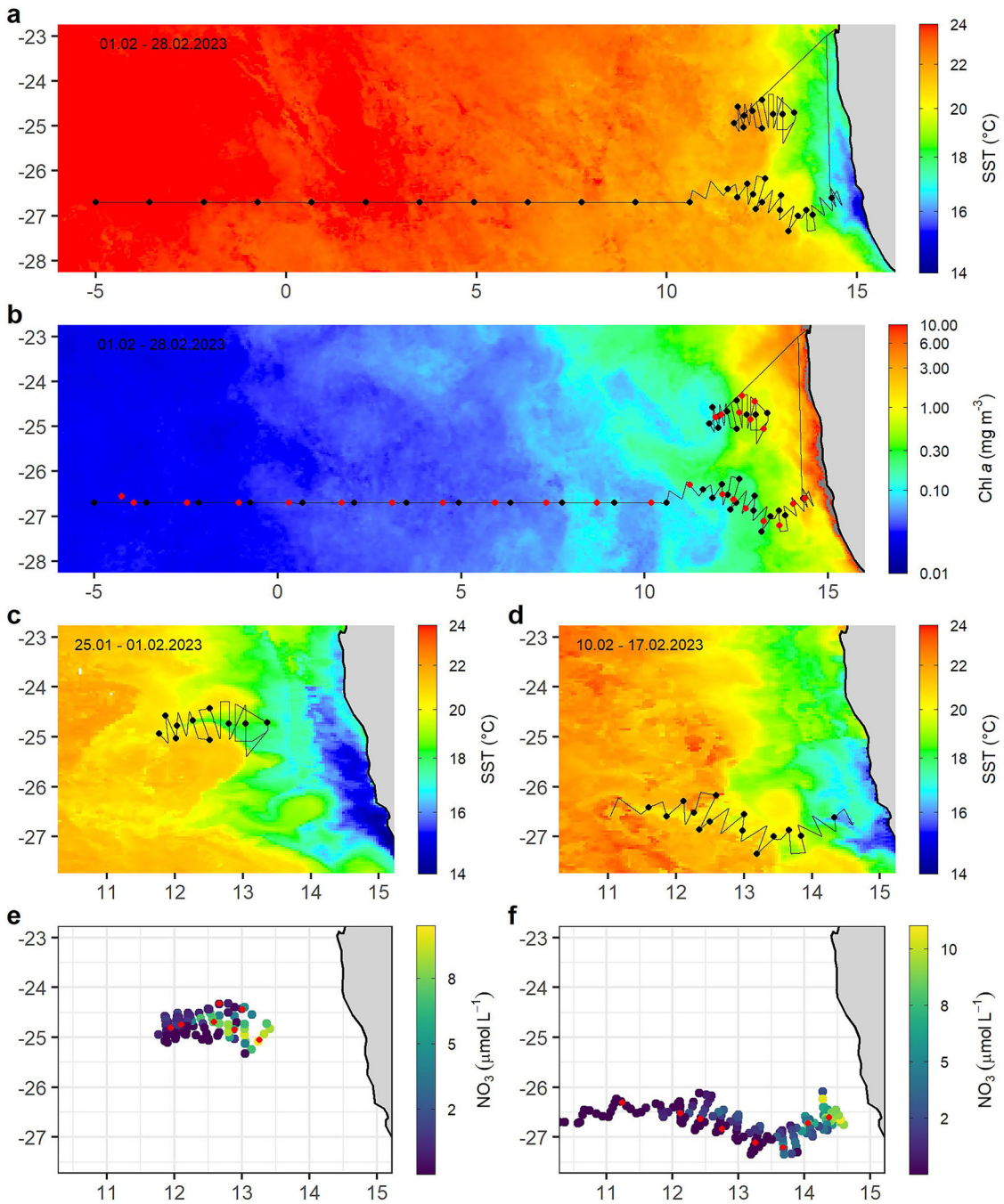

Fig. 1 | Study region and biogeochemical variability. Cruise track (line), sampling stations (black dots for the full study area with a background of **a** SST and **b** Chl *a*. Red dots in 'b' show the locations of bioassay experiments. **c**, **d** Cruise track (line) and sampling stations (black dots) for the two encountered upwelling filaments with a background of SST. **e**, **f** Distribution of surface nitrate concentrations for the two encountered upwelling filaments overlaid with cruise track (lines) and bioassay experiment sites (red dots). Note that all nitrate concentrations outside of the domain shown in panels e-f were <0.06 µmol L^{-1}.

marking the beginning of the PACE mission (ca. 1 year after the research cruise (https://oceandata.sci.gsfc.nasa.gov/l3/) in order to assess satellite-derived nFLH. PACE nFLH data is currently distributed as a 'provisional' data product which has not been validated and may contain significant errors.

Macronutrient concentrations

Macronutrient samples were collected in duplicate using 15 mL acid-washed, pre-rinsed, polypropylene tubes. One aliquot was analysed onboard with a SEAL Analytical QuAAtro segmented flow injection nutrient auto-analyzer and validated against certified reference material (KANSO Technos). The system setup included four channels for nitrate + nitrite (TON), silicic acid, nitrate (NO_3) and phosphate (PO_4). The detection limits for this standard method were 0.005 µmol L^{-1} for silicate, 0.033 µmol L^{-1} for NO_3, and 0.005 µmol L^{-1} for PO_4. The other aliquots were immediately frozen at −20 °C and analysed later in a land-based laboratory using a low-level nanomolar method for NO_3 and PO_4 analyses[30] with a modified version of a SEAL Analytical QuAAtro39 auto-analyser equipped with liquid waveguide capillary cells. Detection limits for this low-level method were NO_3 = 7 nmol L^{-1} and PO_4 = 3 nmol L^{-1}. The low-level method was employed for those samples whose concentrations were initially identified as being below 0.1 µmol L^{-1} for either NO_3 or PO_4 via the standard method.

Chlorophyll and diagnostic phytoplankton pigment concentrations

Samples for Chl *a* were filtered (100–200 mL) onto 25 mm diameter glass microfiber GF/F filters (Fisher MF300), then extracted in the dark for 12–24 h in 10 mL of 90% acetone at −20 °C. The analysis was conducted using a calibrated Turner Designs Trilogy laboratory fluorometer[31].

For phytoplankton pigment analysis, 2–4 L of samples were filtered onto 25 mm diameter GF/F filters (Fisher MF300) and immediately frozen at −80 °C. Once returned to land, pigments were extracted in 90% acetone within plastic vials by homogenizing the filters with glass beads in a cell mill. The mixture was then centrifuged for 10 min at 5200 rpm at 4 °C. The supernatant was filtered through 0.2 µm polytetrafluoroethylene filters (VMR International) and pigment concentrations were quantified using reverse-phase high-performance liquid chromatography (HPLC, Dionex UltiMate 3000 LC system, Thermo Scientific; Van Heukelem and Thomas[32]). Pigment standards were sourced from Sigma-Aldrich and the International Agency for 14 C Determination.

The analysed pigments included Chl *a*, divinyl Chl *a*, Chl *b*, Chl *c*2, Chl *c*3, peridinin, 19'-butanoyloxyfucoxanthin, fucoxanthin, violaxanthin, 19'-hexanoyloxyfucoxanthin, diatoxanthin, alloxanthin, zeaxanthin, neoxanthin, and combined α-carotene and β-carotene. These pigments were used to determine the relative abundance of 10 phytoplankton groups via CHEMTAX, utilizing published field-derived starting pigment ratios[33,34]. The distinguished classes of phytoplankton were diatoms, dinoflagellates, *Synechococcus*, high-light (HL) and low-light (LL) *Prochlorococcus*, haptophytes, pelagophytes, prasinophytes, cryptophytes, and chlorophytes. Of these, seven classes (diatoms, dinoflagellates, *Synechococcus*, Prochlorococcus, haptophytes, pelagophytes and prasinophytes) dominated contributions and are presented here. There are likely uncertainties with CHEMTAX derived phytoplankton groups[35–37], therefore subsequent data analyses was conducted using both CHEMTAX-derived groups as well as directly with diagnostic pigments (Fig. S4).

Nutrient addition bioassay experiments

A total of 27 nutrient amendment bioassay experiments were conducted following protocols described in ref. 24. Surface seawater was collected via the tow-fish 1–2 h after sunset. Samples were collected into either 0.5 L or 1 L trace-metal-clean Nalgene polycarbonate bottles. An initial measurement of Chl *a* concentration was taken, and then bottles were spiked in triplicate with Fe, N and Fe + N. Fe was added as $FeCl_3$ to a final amended concentration of 2 nM and N was added as a combined addition of 1 µM NO_3 and 1 µM ammonium. NO_3 and ammonium stocks were pre-cleaned to remove contaminating trace metals by passing solutions through a column of a metal-chelating resin (Chelex, Bio-Rad). Initial conditions and triplicate control bottles with no nutrients added were also collected alongside all treatment experiments. Bottles were placed on the back deck of RV Meteor in incubators connected to the ship´s underway flow-through system to maintain temperatures in the incubators similar to sea surface waters. We note that our cruise track crossing the filaments led to temperature changes (maximum of ca. 3 °C) in the incubators over the experimental duration (i.e., cooling on crossing the filament, warming on exiting the filament), but consider that overall chlorophyll and active fluorescence changes between control and nutrient amended samples (both incubated under identical conditions) will be robust to such variability. Incubators were equipped with Blue Lagoon screening (Lee Filters), which maintained irradiance ~30% compared to the sea surface. Samples were incubated for ~48 h and sampled for Chl *a* concentration and active fluorescence measurements (see below). Sites were characterized as either Fe or N limited based on statistically significant (ANOVA followed by Tukey HSD test) increases in Chl *a* concentrations in nutrient-amended samples relative to untreated controls.

Phytoplankton absorption

Hyperspectral absorption coefficients in the visible spectrum (λ = 400–700 nm) were measured in triplicate using a point-source integrating cavity absorption meter, PSICAM[38,39]. The PSICAM uses a halogen lamp (Illumination Technologies CF1000e) as the light source and a spectrometer (Aventes AvaSpec ULS 2048XL-RS-EVO) as the detector. The instrument was calibrated using a nigrosin solution with a maximum absorption coefficient of ~0.5 m^{-1}. Milli-Q Ultrapure water was used as a reference for both the calibration and sample measurements. Samples were analysed for both total absorption (a_{tot}) and color dissolved organic material absorption (a_{cdom}). The a_{cdom} measurement was obtained after samples were filtered through 0.2 µm pore size Whatman Nuclepore™ track-etched membrane filters. Phytoplankton absorption coefficients (a_{ph}) were estimated as the difference between the measured a_{cdom} and a_{tot} with the assumption of minimal absorption by other particles.

Active fluorescence measurements

A single-turnover active fluorometer (LabSTAF, Chelsea Technologies Ltd, UK) was used for all measurements of variable active Chl *a* fluorescence. Samples were collected several hours after sunset and kept in the dark at sea surface temperature before analysis. Fluorescence induction transients were induced with a 100 µs light pulse at 452 nm. Excitation pulse intensity was automatically adjusted to ensure optimal saturation of the fluorescence transient. Measurements were conducted for 100 s and average values from the last 30 s were used. No increase in maximum fluorescence (F_m) was observed during the 100 s of measurements, indicating that relaxation of reversible non-photochemical quenching did not affect the derived values. Blank measurements of 0.2 µm filtrate were conducted at a subset of samples. Blank values of Chl *a* fluorescence were consistently <3% of the corresponding Fm and therefore no blank correction was applied to the data. Values of F_m were normalized to the corresponding Chl *a* concentration to generate a value of F/Chl^{active}. Chl *a* was not converted to phytoplankton absorption using an empirical relationship (see Section 'Above-water Radiometry' and Fig. S2), as such relationships are generated with data originating from broad ecological gradients that likely do not well reflect chlorophyll-absorption relationships following short-term nutrient additions (dominated by increased chlorophyll biomass with more restricted changes in phytoplankton size structure).

Above-water radiometry

A system with two sets of TriOS RAMSES spectroradiometers on a custom-built frame with an extending arm was installed at the bow of RV Meteor at a height ~7.7 m above the sea surface. Each set consisted of an ACC hyperspectral irradiance meter and two ARC hyperspectral radiance meters with a 7° field-of-view. The RAMSES-ACC hyperspectral irradiance meter measured the total downwelling irradiance $E_S(\lambda)$, with PAR calculated as the sum of $E_D(\lambda = 400 - 700\,\mathrm{nm})$. The two RAMSES-ARC radiometers were positioned at nadir angles of 45° and 90° to obtain total upwelling sea surface radiance L_T (θ_T, Φ, λ) and sky leaving radiance $L_{sky}(\theta_{sky}, \Phi, \lambda)$, respectively. The two sets of radiometers were positioned at relative azimuth angles of 45° from the direction of the ship and 90° between them. This allowed for the routine selection of the radiometer set with the best azimuth angle from the sun and thus with the lowest impact from surface reflectance glint[29].

Hyperspectral (λ = 320–900 nm) radiometric quantities were recorded underway at 5-min intervals. Water leaving radiance (L_w) and remote-sensing reflectance (R_{rs}) were calculated using

$$R_{rs} = \frac{L_w}{E_D} = \frac{L_t - \left(\rho_{air-sea} * L_{sky}\right)}{E_D} \quad (3)$$

multiple surface reflected glint corrections were applied and visually compared for every timepoint following proposed guidelines[40,41] with the best approximations derived using Gould et al.[42]. Fluorescence line height (FLH) was then calculated from L_w using the approximate central wavelengths of

the corresponding MODIS-Aqua wavebands as shown below.

$$FLH = L_{678} - \left(\frac{\lambda_{748} - \lambda_{678}}{\lambda_{748} - \lambda_{667}}\right) L_{667} - \left(1 - \frac{\lambda_{748} - \lambda_{678}}{\lambda_{748} - \lambda_{667}}\right) L_{748} \quad (4)$$

where $\lambda_{678}, \lambda_{667}, \lambda_{748}$ represent the wavelengths of the fluorescence band and two baseline bands respectively, and L_{678}, L_{667}, L_{746} are the corresponding water leaving radiances.

Radiometric Chl *a* was derived from R_{rs} using the NASA OC3 blue-green band ratio algorithm[43,44]. These values were then compared with discrete samples taken during the research cruise. These comparisons showed strong agreement between the methods, with radiometric Chl *a* correlating well with both HPLC-derived Chl a concentrations ($R^2 = 0.698$, $p < 0.001$, $n = 68$) and acetone-extracted fluorometric measurements ($R^2 = 0.691$, $p < 0.001$, $n = 68$), albeit with slight offsets for the two methods of chlorophyll-a concentration determination (Fig. S1). When the dataset was restricted to samples with Chl *a* concentrations <1 mg m^{-3}, the relationships slightly improved (HPLC: $R^2 = 0.710$, $p < 0.001$, $n = 62$; acetone-extracted fluorometry: $R^2 = 0.715$, $p < 0.001$, $n = 62$), suggesting especially strong consistency at lower concentrations common throughout most of the open ocean.

Values of FLH derived from the field radiometry were normalized to phytoplankton absorption (a_{ph}) to generate a shipboard estimate of absorption-normalized, sunlight stimulated (passive) Chl *a* fluorescence ($F/a_{ph}^{passive}$). To estimate a_{ph} at the required resolution, we used an empirical relationship between in situ TChl *a* (Chl *a* + divinyl Chl *a*) and spectrally integrated phytoplankton absorption based on data from this study and a much larger dataset (the BENCAL dataset from Bricaud et al.[45]), which was collected in the Benguela-South Atlantic region (Fig. S2). Spectrally integrated a_{ph} was weighted to a measured clear-sky E_D (i.e., $\sum_{(400-700)} a_{ph}(\lambda) * E_D(\lambda) / \sum_{(400-700)} E_D(\lambda)$) to reflect light absorbed by phytoplankton under ambient surface sunlight conditions. This region-specific relationship was then applied to convert radiometer-derived TChl *a* to a_{ph}. Although the relationship between Chl *a* and a_{ph} is typically indistinguishable from linear correlation at very low Chl *a* concentrations, this does not hold for the full range of Chl a concentrations encountered in our study region. to Chl *a* concentrations, normalizing FLH to a_{ph} derived from a region-specific algorithm, rather than to TChl *a* alone, provides a more physiologically relevant metric of passive fluorescence yield, as it accounts for variability in pigment packaging (i.e., specifically accounting for the absorbed energy that could go on to stimulate fluorescence rather than the concentration of total Chl *a* pigment; Bricaud et al.[46]). We note that a potential improvement in our method could be to estimate phytoplankton absorption directly using the shipboard radiometric signals and other underway shipboard measurements alongside satellite algorithms for derivation of a_{ph} (e.g., McKinna and Werdell[45]).

To analyse $F/a_{ph}^{passive}$ as a function of irradiance, daily $F/a_{ph}^{passive}$ vs. PAR curves were created based on PAR binned averages of $F/a_{ph}^{passive}$. A non-linear regression model was fit to the data[4,47] using the nls package from R[48].

$$F/a_{ph}^{passive} = F/a_{ph_{max}}^{passive} * \tan h\left(\frac{\alpha_f * PAR}{F/a_{ph_{max}}^{passive}}\right) \quad (5)$$

where $F/a_{ph_{max}}^{passive}$ is the maximum light-saturated absorption-normalized passive fluorescence and α_f corresponds to the initial, light-limited slope of the curve. The PAR intensity where $F/a_{ph}^{passive}$ approaches saturation was defined as E_{kf} and is described as $F/a_{ph_{max}}^{passive}/\alpha_f$. Values of $F/a_{ph_{max}}^{passive}$, α_f, and E_{kf} were extracted for each day (with each day corresponding to one $F/a_{ph}^{passive}$ versus PAR curve) and used for comparison with ancillary data. Iterative confidence intervals for both the model fits and extracted parameters were also generated.

Only radiometric data collected when the ship was on station (i.e., not moving) were used in this study, which corresponded to the location of discrete collected samples and characterization of the physical structure of the upper water column. To address outlying data for $F/a_{ph}^{passive}$ versus irradiance curves, each daily set of observations was fitted with a second-order polynomial using a robust regression method proposed by Schallenberg et al.[4]. The fitted values represent the model-predicted $F/a_{ph}^{passive}$ generated from this regression. Deviations between observed and fitted values were expressed as residuals, which were standardized on a daily basis by calculating Z-scores (residual minus daily mean, divided by the daily standard deviation). Observations with standardized residuals exceeding a threshold (Zc) were identified as outliers. A threshold of $Z_C = 2$ provided the closest agreement with visual inspection of the daily curves and was therefore applied consistently throughout the dataset. This procedure resulted in 2.62% of observations being classified as outliers.

Results and discussion

Physical and biogeochemical setting of the study region

Major gradients in sea surface temperatures, nutrient concentrations, and phytoplankton biomass and community structure were observed between the Benguela upwelling region and the South Atlantic Subtropical Gyre, in agreement with previous studies[27,49–51]. During the observation period (28.01.2023–03.03.2023), active near-coastal upwelling was maintained, as indicated by lower average SSTs near the coast (>13°E, SST = 17.68 ± 2.13 °C), which increased progressively towards the subtropical gyre (<13°E, SST = 21.29 ± 1.38 °C; Fig. 1a, c, d). Surface waters in the upwelling zone and filaments were characterized by elevated concentrations of NO_3 and PO_4 (up to 11 µmol L^{-1} and 1.40 µmol L^{-1}, respectively), while offshore surface waters of the subtropical gyre were depleted, with maximum concentrations of 0.14 µmol L^{-1} and 0.20 µmol L^{-1} for NO_3 and PO_4 respectively (Fig. 1e, f). In contrast, silicic acid exhibited a less consistent spatial decline and remained relatively elevated offshore (1.15–1.95 µmol L^{-1}). Surface Chl *a* concentrations were 8–10 times higher in macronutrient-rich regions nearer the coast (mean = 0.56 ± 1.17 mg m^{-3}, max = 6.83 mg m^{-3}) compared to oligotrophic subtropical gyre waters (mean = 0.03 ± 0.02 mg m^{-3}, max = 0.10 mg m^{-3}; Fig. 1b), reflecting the transition from enhanced phytoplankton productivity associated with upwelled nutrient supply near the coast to the highly stratified waters of the subtropical gyre.

Active fluorescence response to nutrient limitation

A total of 27 controlled nutrient-addition bioassay experiments were conducted throughout the cruise to unambiguously diagnose the nutrient limitation status of the extant phytoplankton community. The results showed transitions from Fe limitation in waters with residual NO_3 concentrations to N limitation in waters where NO_3 was depleted (as shown by increases in chlorophyll-a in response to nutrient supply), in agreement with a previous study[24]. Using this large experimental data set, we found that an initial seawater threshold NO_3 concentration of 0.06 µmol L^{-1} was effective in distinguishing N limited sites from Fe limited sites in this region (Fig. 2a). Subsequently, surface NO_3 concentration measurements, which had a much higher spatial-temporal resolution than the bioassay experiments, were used to classify surface waters as either Fe or N limited.

In experiments where N was diagnosed as the limiting nutrient, Chl a-normalized maximum active fluorescence was relatively low and the supply of Fe led to no significant changes, whereas N addition on average led to small increases (Fig. 2b). The small increases in response to N addition resulted from occasionally switching the initially N limited phytoplankton into Fe limitation, as has been previously shown for nutrient addition bioassay experiments (Behrenfeld et al.,[52]; Browning et al.,[24]). In contrast, in experiments where Fe limitation was identified, Chl *a*-normalized maximum active fluorescence was elevated in non-nutrient amended controls and N-amended treatments and declined on average >2-fold following Fe supply (Fig. 2b; note that maximum active fluorescence was not normalized to phytoplankton absorption, as this was not determined in the experimental samples and in situ absorption versus Chl *a* datasets (e.g., Fig. S2)

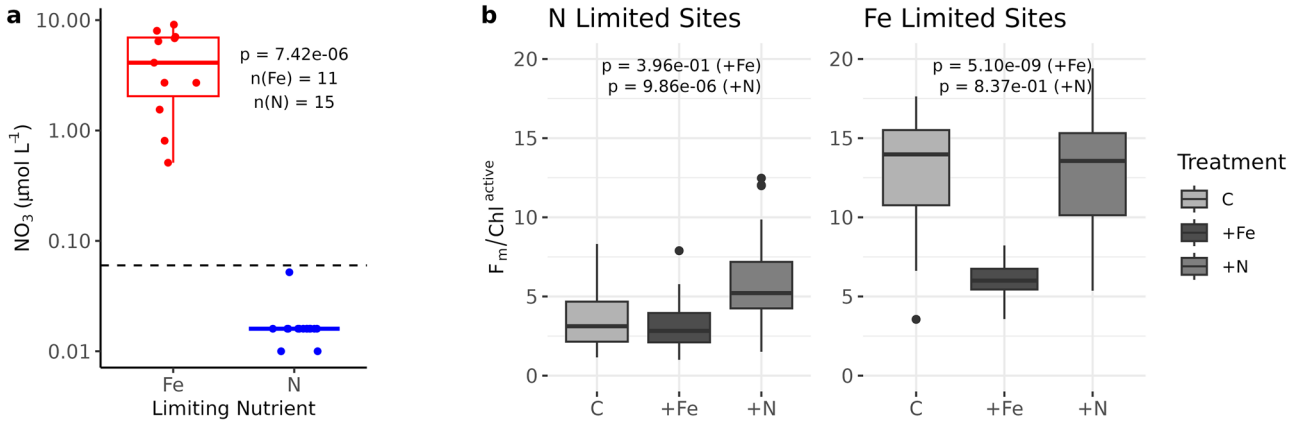

Fig. 2 | Response of Chl *a*-normalized maximum active fluorescence to N or Fe limited conditions. a NO_3 concentrations measured at experimental start points that were classified as either Fe (elevated NO_3) or N (depleted NO_3) limited. The dashed line shows the regionally-defined NO_3 concentration division between N and Fe limited sites (0.06 μmol L^{-1}). Sample sizes (n) and p-values are based on non-parametric Wilcoxon rank-sum tests comparing the two groups. **b** Box and whisker plot showing Fm/Chl^{active} results for experimental treatments with Fe added ("+Fe"), N added ("+N") or without additions ("C") for all N limited sites (left) and all Fe limited sites (right). Dots show outlier data and error bars indicate the standard deviation. Two-sided, unpaired t-test p values for significantly different means is shown for addition experiments (either Fe or N addition) compared to the control (for Fe limited sites, $n = 28$ for C and $n = 30$ for +Fe and +N; for N limited sites, $n = 39$ for all; C, +Fe and +N).

reflect broad geographical shifts in phytoplankton ecophysiology that likely poorly capture the short-term response of the incubated phytoplankton community). The rapid (48 h) reductions in Chl-normalized maximum active fluorescence following Fe addition are likely to be due to nutrient-regulated changes in the relative abundance and energetic coupling of photosynthetic electron transport chain components and light-harvesting pigment-protein complexes. Specifically, under Fe limited conditions, phytoplankton exhibit a reduction in photosystem I (PSI) abundance relative to photosystem II (PSII), due to the elevated Fe requirement of PSI over PSII[53–55]. As fluorescence emission from PSI at 685 nm is extremely low, relative to PSII, this enhanced PSII:PSI can result in enhanced Chl *a* -normalized fluorescence. Additionally, Fe limitation has been demonstrated to cause increased energetic uncoupling of some proportion of the pigment-protein complexes from reaction centers in the membrane, which results in elevated fluorescence yields[3,22,52,56]. Following Fe supply, both rapid reductions in PSII:PSI together with an increased energetic coupling of pigment-protein complexes to reaction centers are then thought to drive the observed Chl *a*-normalized active fluorescence reductions[3,11,22].

Variability in passive fluorescence

Field observations of passive, sunlight-stimulated Chl fluorescence have demonstrated increases at low irradiances followed by a general transition to a fluorescence plateau at higher irradiances[4,5,57,58]. The light-saturated fluorescence plateau is the result of increasing absorbed excitation energy being balanced by an increase in absorbed energy dissipated as heat (referred to as non-photochemical quenching, NPQ)[5,10]. This plateau corresponds to the majority of satellite-retrieved passive Chl fluorescence data, as these are acquired around midday under conditions of maximum sunlight[5,10,12]. Of the 26 days of observations during the research cruise, 22 had sufficiently high light levels (i.e., PAR > 500 μmol photons m^{-2} s^{-1}), while on station, to generate absorption-normalized passive fluorescence $F/a_{ph}^{passive}$ curves (Fig. 3a, b and S1), and in all cases high light plateaus in $F/a_{ph}^{passive}$ were observed (Fig. S3).

The light-saturated maximum from $F/a_{ph}^{passive}$ versus irradiance curves, $F/a_{ph_{max}}^{passive}$, was subsequently evaluated in the context of potential environmental and ecological drivers (Figs. 3–5). Consistent with the observations made by active fluorometry, $F/a_{ph_{max}}^{passive}$ showed a substantial and significant difference between Fe and N limited waters (Fig. 3), with Fe-limited stations on average exhibiting 3.1-fold higher values (mean ± SD = 5.03 ± 1.45 mW m^{-1} sr^{-1} nm^{-1}) compared to N-limited waters (1.59 ± 0.66 mW m^{-1} sr^{-1} nm^{-1}; Kruskal-Wallis $p < 0.001$). A strong positive correlation was also observed with surface NO_3 concentrations that was previously identified as a reliable index of Fe versus N limitation (Fig. 4a). The fold difference in $F/a_{ph_{max}}^{passive}$ between Fe and N limited sites is consistent with previous findings in the tropical Pacific, where a ca. 3-fold difference in Chl-normalized passive fluorescence was observed[5]. However, in strong contrast to the tropical Pacific study, we here encountered major variability in the physics (temperatures, mixing, and light climate) and biogeochemistry (phytoplankton abundance and community structure) of the upper water column alongside the transitions between Fe and N limitation.

To evaluate the impact of upper water column physical characteristics on passive fluorescence, three key parameters were examined: SST, MLD, and $\widetilde{E}_g$. A significant negative correlation was found between SST and $F/a_{ph_{max}}^{passive}$ (Fig. 4b). This correlation is most likely influenced by the distribution of nutrient limitation conditions (Fe limitation in colder, high NO_3, upwelled waters and N limitation in warmer, low NO_3 subtropical gyre waters; Fig. 1e, f). Impacts of SST on passive fluorescence emission (e.g., direct temperature-driven regulation of photosynthetic rates and thus phytoplankton ecophysiology) cannot be ruled out based on the observations from this study. However, the results of the nutrient addition bioassay experiments strongly suggest SST being correlative with $F/a_{ph_{max}}^{passive}$ and not a causative driver. Specifically, in the bioassay experiments only nutrient availability was changed with temperature remaining constant for all treatments; as previously discussed, in these experiments, Chl-normalized maximum active fluorescence declined on average >2-fold following Fe addition in Fe limited waters, similar to the fold differences in $F/a_{ph_{max}}^{passive}$ between Fe and N limited sites. A general deepening of the MLD was observed offshore alongside no clear change in $\widetilde{E}_g$ with neither showing a statistically significant relationship with $F/a_{ph_{max}}^{passive}$ (Fig. 4c, d). This suggested that neither $\widetilde{E}_g$ nor light variability (characterized by MLD) were dominant drivers of $F/a_{ph_{max}}^{passive}$ in this region.

Phytoplankton community composition has been shown to be important in influencing active fluorescence signals[2,7] and could play a strong role in modulating sunlight-stimulated passive fluorescence. This is due to different phytoplankton taxa varying widely in composition and arrangement of light harvesting pigments as well as photoprotective strategies[2,7]. Correlation analyses of $F/a_{ph_{max}}^{passive}$ with phytoplankton community structure derived from diagnostic pigment and CHEMTAX analyses showed several significant trends (Figs. 5 and S2). The estimated contribution of diatoms to TChl *a* correlated positively and significantly

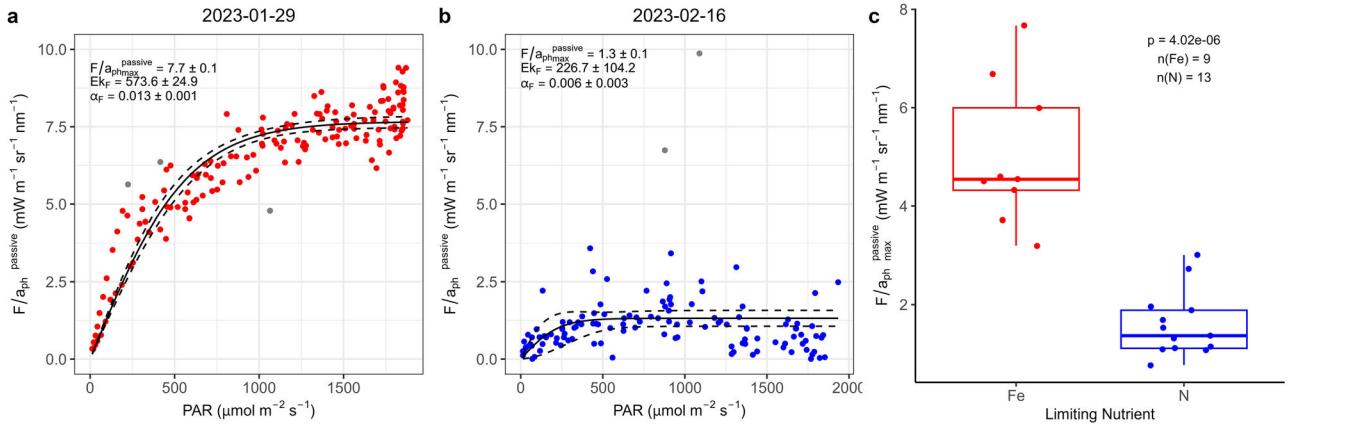

Fig. 3 | Nutrient regulation of light-saturated, absorption-normalized passive fluorescence. $F/a_{ph}^{passive}$ versus photosynthetically active radiation (PAR) response curves derived from the shipboard radiometry for two example days (29.01.2023 and 16.02.2023) at **a** Fe limited and **b** N limited sites. Dots indicate PAR-binned averages of $F/a_{ph}^{passive}$, with lines indicating model fits following Eq. 5. Corresponding values of $F/a_{ph}^{passive}$, E_{kf}, and α_f from the model fits are shown. Solid lines are model fits with 95% confidence bands shown as dashed lines. **c** Box and whisker plot showing $F/a_{ph}^{passive}$ for Fe-limited (red) and N-limited (blue) sites. A non-parametric Wilcoxon rank-sum test comparing the two limiting nutrient groups was performed with corresponding p value shown.

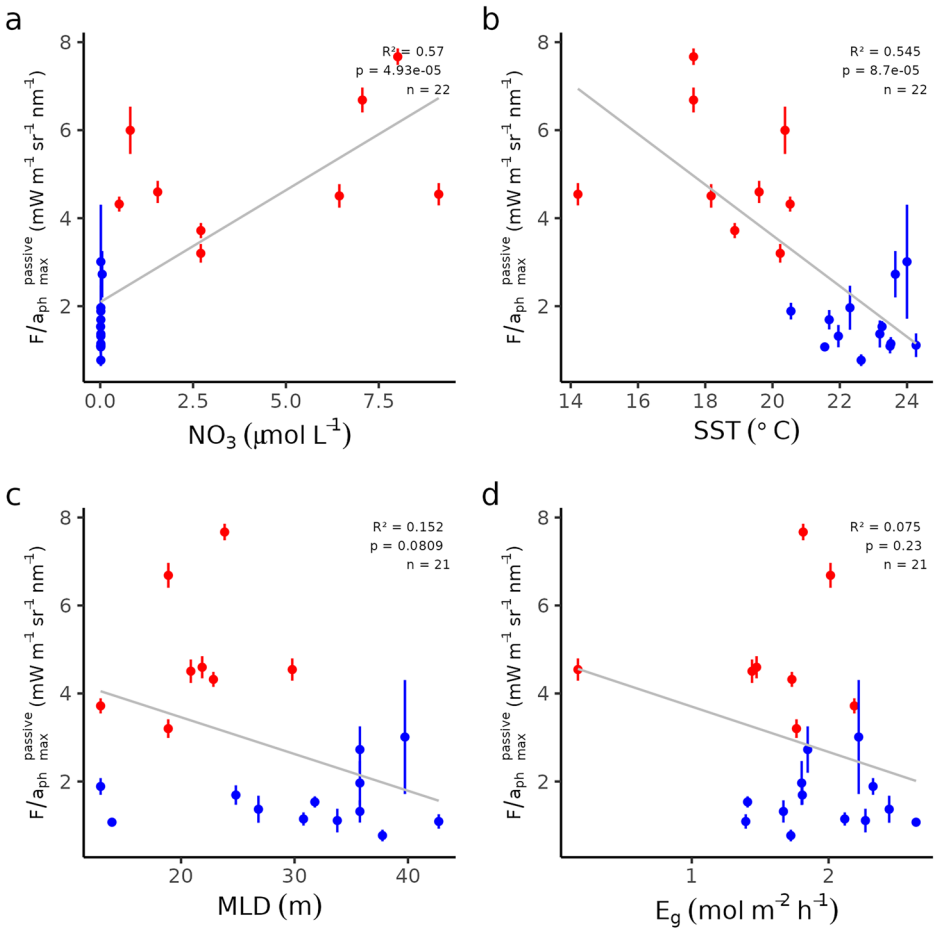

Fig. 4 | Relationships between maximum, absorption-normalized passive fluorescence $F/a_{ph_{max}}^{passive}$ and environmental variables. Each point represents a daily $F/a_{ph_{max}}^{passive}$ value with model fit confidence intervals (error bars), derived from model fits of $F/a_{ph}^{passive}$ versus PAR (Eq. 5) (Fig. 3a, b and S1). Panels show correlations with **a** NO_3 concentration, **b** sea surface temperature, **c** mixed layer depth, and **d** median mixed layer irradiance. Red and blue colors indicate locations that were determined as Fe- and N-limited, respectively.

with $F/a_{ph_{max}}^{passive}$ ($R^2 = 0.56$, $p < 0.001$, $n = 21$; Fig. 5a) whilst correlations with the estimated contributions of *Prochlorococcus* and *Synechococcus* were significant and negative ($R^2 = 0.67$, $p < 0.001$, $n = 21$ for *Prochlorococcus* and $R^2 = 0.74$, $p < 0.001$, $n = 21$ for *Synechococcus*; Fig. 5c, d). Correlations with the contributions of dinoflagellates, haptophytes, pelagophytes, and prasinophytes were not significant. Similar correlations were also found with Chl-normalized pigments diagnostic of the various phytoplankton groups (Fig. S4).

Overall, these trends resulted from the broadscale shifts from diatom-dominated communities in colder, higher NO_3, Fe limited waters in the Benguela upwelling through to cyanobacteria-dominated communities in warmer, lower NO_3, N limited waters of the subtropical gyre. As for SST, whilst we cannot unambiguously rule out the role of such taxonomic shifts in (co-)driving the trends in $F/a_{ph_{max}}^{passive}$, the nutrient addition bioassay experiments strongly suggested physiological changes were more important than taxonomic shifts. Specifically, whilst strong shifts in phytoplankton

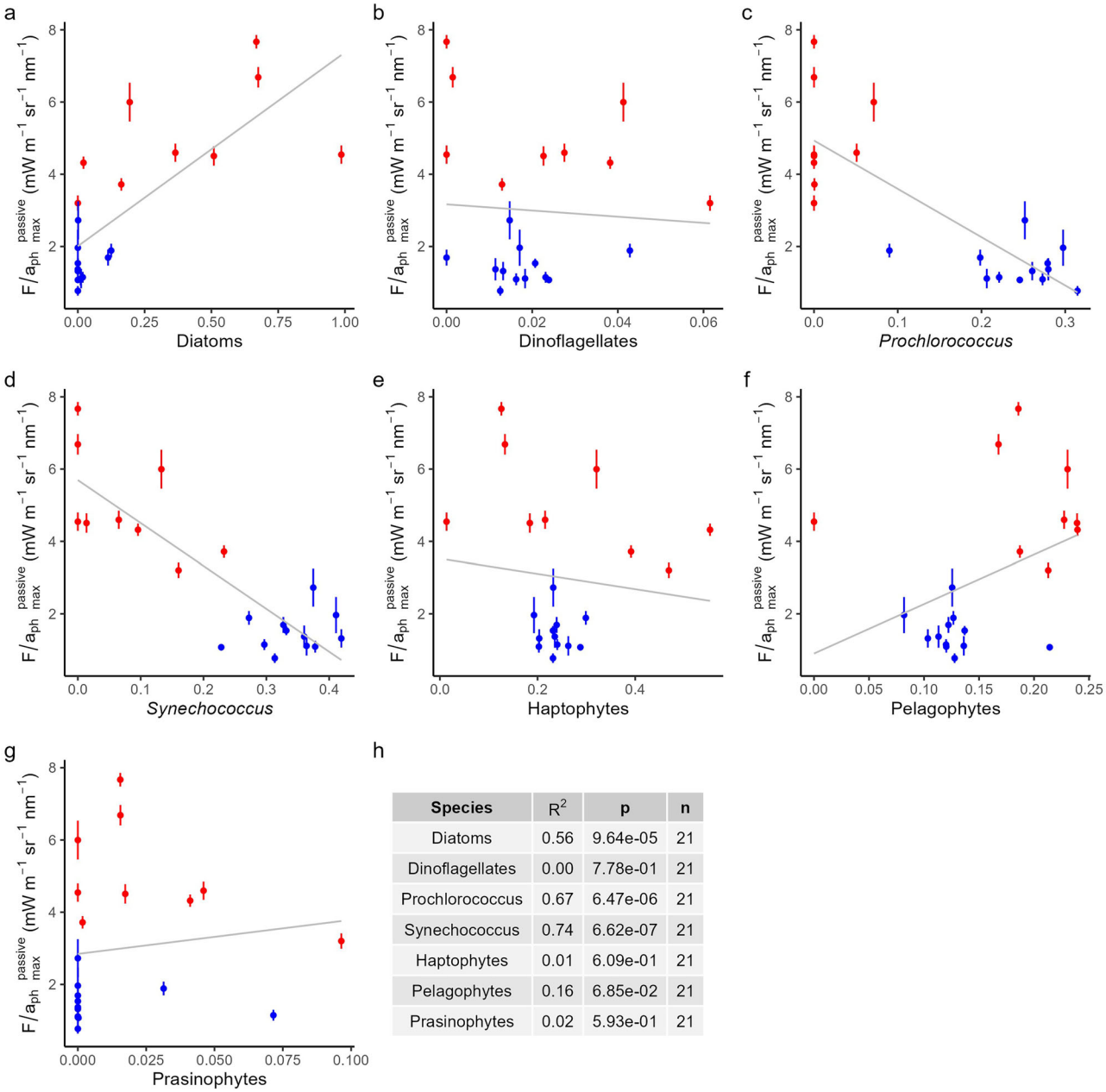

Species	R^2	p	n
Diatoms	0.56	9.64e-05	21
Dinoflagellates	0.00	7.78e-01	21
Prochlorococcus	0.67	6.47e-06	21
Synechococcus	0.74	6.62e-07	21
Haptophytes	0.01	6.09e-01	21
Pelagophytes	0.16	6.85e-02	21
Prasinophytes	0.02	5.93e-01	21

Fig. 5 | Relationships between maximum, absorption-normalized passive fluorescence, $F/a_{ph}^{passive}_{max}$, and the estimated contribution of phytoplankton classes to total Chl *a*. **a**–**g** Each point represents a daily $F/a_{ph}^{passive}_{max}$ value with model fit confidence intervals (error bars), derived from model fits of $F/a_{ph}^{passive}$ to PAR (Eq. 5). As for Fig. 4, red and blue points represent locations determined as Fe- and N-limited, respectively. Statistical results are shown in (**h**).

community structure have previously been observed in this region over short experimental timescales (48 h)[24], the observed community shifts following supply of the limiting nutrient (a ubiquitous increase in the contribution of diatoms) were in the opposite direction to that observed here in the correlation analyses between $F/a_{ph}^{passive}_{max}$ and community structure. That is, we found experimental supply of Fe (i.e., reducing Fe stress) led to on average >2-fold reductions of F/Chl^{active} at Fe limited sites (Fig. 2a), despite expected (community structure changes within bioassays were not evaluated) increases in the contribution of diatoms to the community[24]; this is opposite to the positive in situ correlation between $F/a_{ph}^{passive}_{max}$ and diatom contribution (Fig. 5a). Therefore, whilst acknowledging that this interpretation assumes that active and passive fluorescence signals would change in the same direction to a given change in community structure, we conclude that the significant observed relationships between $F/a_{ph}^{passive}_{max}$ and community structure were not causative, but correlative, a result of the broad-scale covariation of shifts from Fe to N limitation and diatoms to cyanobacteria in the study region.

Our results provide field-validated data for assessing whether patterns in $F/a_{ph}^{passive}_{max}$ detected remotely via satellite could serve as a tracer of nutrient limitation at broad geographic and temporal scales. Inspection of MODIS-derived nFLH and nFLH/a_{ph} (with a_{ph} derived from the same regional relationship applied to the shipborne radiometry data; Fig. S2) for the time of our research cruise displayed noisy (that is high pixel-to-pixel variability) signals at the small time and spatial scales required for observing dynamic filaments (Fig. S5), which is a known issue with MODIS fluorescence line height data[59,60]. The recent launch of the higher performance Plankton, Aerosol, Cloud, ocean Ecosystem (PACE) sensor may allow for signals to be detected at the required resolutions[61]. PACE was launched ca. 1 year after our research cruise and therefore data corresponding to our field occupation are not available; however, provisional PACE data captured

shortly after launch in the same season show promise, with elevated nFLH/a_{ph} observable in low SST filament structures relative to background conditions (Fig. S6), strongly resembling our shipboard observations (Fig. 3).

Conclusion

Combining shipborne above-water radiometry with physical-biogeochemical characterization of the surface ocean in the southeast Atlantic Ocean we found a ca. 3-fold variability in light saturated, absorption-normalized passive Chl *a* fluorescence ($F/a_{ph}^{passive}_{max}$), which could be explained by transitions between N and Fe limited conditions. Alongside comparable, short-term changes in Chl *a*-normalized maximum active fluorescence measured in response to Fe or N supply in bioassay experiments, our results suggested that surface ocean mixing depths, light climate, and phytoplankton community structure were secondary factors in regulating broadscale gradients in $F/a_{ph}^{passive}_{max}$. In line with previous observations in the tropical Pacific[5], our study further supports the potential for utilization of these signals to reveal nutrient limitation regimes at global, high frequency scales[5,10]. We suggest that further studies in other oceanographic regions that directly link passive fluorescence with a full range of potential drivers, as conducted here, will be key in paving the way towards confident utilization of these satellite data.

Data availability

Above water radiometric data are available at https://doi.org/10.1594/PANGAEA.973430. Level 3 satellite MODIS and PACE products can be accessed at https://oceandata.sci.gsfc.nasa.gov/l3/. All analyses were performed using R Statistical Software (v4.5.2; R Core Team 2025).

Received: 30 June 2025; Accepted: 25 November 2025;
Published online: 07 December 2025

References

1. Huot, Y. & Babin, M. in *Chlorophyll a fluorescence in aquatic sciences: Methods and applications* 31-74 (Springer, 2010).
2. Proctor, C. W. & Roesler, C. S. New insights on obtaining phytoplankton concentration and composition from in situ multispectral Chlorophyll fluorescence. *Limnol. Oceanogr. Methods* **8**, 695–708 (2010).
3. Schrader, P. S., Milligan, A. J. & Behrenfeld, M. J. Surplus photosynthetic antennae complexes underlie diagnostics of iron limitation in a cyanobacterium. *PloS ONE* **6**, e18753 (2011).
4. Schallenberg, C., Lewis, M. R., Kelley, D. E. & Cullen, J. J. Inferred influence of nutrient availability on the relationship between sun-induced chlorophyll fluorescence and incident irradiance in the Bering Sea. *J. Geophys. Res. Oceans* **113**, C7 (2008).
5. Browning, T. J. et al. Persistent equatorial Pacific iron limitation under ENSO forcing. *Nature* **621**, 330–335 (2023).
6. Huot, Y., Antoine, D. & Vellucci, V. Daily Sun-induced chlorophyll fluorescence vs. irradiance curves reflect the photoadaptation of phytoplankton in surface waters. *Limnol. Oceanogr.* **11**, 1–15 (2025).
7. Suggett, D. J., Moore, C. M., Hickman, A. E. & Geider, R. J. Interpretation of fast repetition rate (FRR) fluorescence: signatures of phytoplankton community structure versus physiological state. *Mar. Ecol. Prog. Ser.* **376**, 1–19 (2009).
8. Cullen, J. J., Yentsch, C. M., Cucci, T. L. & MacIntyre, H. L. in *Ocean optics IX*. 149-156 (SPIE, 1988).
9. Babin, M., Morel, A. & Gentili, B. Remote sensing of sea surface sun-induced chlorophyll fluorescence: consequences of natural variations in the optical characteristics of phytoplankton and the quantum yield of chlorophyll a fluorescence. *Int. J. Remote Sens.* **17**, 2417–2448 (1996).
10. Behrenfeld, M. J. et al. Satellite-detected fluorescence reveals global physiology of ocean phytoplankton. *Biogeosciences* **6**, 779–794 (2009).
11. Behrenfeld, M. J. & Milligan, A. J. Photophysiological expressions of iron stress in phytoplankton. *Annu. Rev. Mar. Sci.* **5**, 217–246 (2013).
12. Letelier, R. M. & Abbott, M. R. An analysis of chlorophyll fluorescence algorithms for the Moderate Resolution Imaging Spectrometer (MODIS). *Remote Sens. Environ.* **58**, 215–223 (1996).
13. Huot, Y., Brown, C. A. & Cullen, J. J. New algorithms for MODIS sun-induced chlorophyll fluorescence and a comparison with present data products. *Limnol. Oceanogr. Methods* **3**, 108–130 (2005).
14. Gower, J. Observations of in situ fluorescence of chlorophyll-a in Saanich Inlet. *Bound.-Layer. Meteorol.* **18**, 235–245 (1980).
15. McClain, C. R., Franz, B. A. & Werdell, P. J. Genesis and evolution of NASA's satellite ocean color program. *Front. Remote Sens.* **3**, 938006 (2022).
16. Browning, T. J. & Moore, C. M. Global analysis of ocean phytoplankton nutrient limitation reveals high prevalence of co-limitation. *Nat. Commun.* **14**, 5014 (2023).
17. Moore, C. M. et al. Iron limits primary productivity during spring bloom development in the central North Atlantic. *Glob. Change Biol.* **12**, 626–634 (2006).
18. Browning, T. et al. Nutrient regimes control phytoplankton ecophysiology in the South Atlantic. *Biogeosciences* **11**, 463–479 (2014).
19. Kolber, Z. S. et al. Iron limitation of phytoplankton photosynthesis in the equatorial Pacific Ocean. *Nature* **371**, 145–149 (1994).
20. Geider, R. J., La Roche, J., Greene, R. M. & Olaizola, M. Response of the photosynthetic apparatus of Phaeodactylum tricornutum (Bacillariophyceae) to nitrate, phosphate, or iron starvation 1. *J. Phycol.* **29**, 755–766 (1993).
21. Schallenberg, C., Strzepek, R. F., Bestley, S., Wojtasiewicz, B. & Trull, T. W. Iron limitation drives the globally extreme fluorescence/chlorophyll ratios of the Southern Ocean. *Geophys. Res. Lett.* **49**, e2021GL097616 (2022).
22. Macey, A., Ryan-Keogh, T., Richier, S., Moore, C. & Bibby, T. Photosynthetic protein stoichiometry and photophysiology in the high latitude North Atlantic. *Limnol. Oceanogr.* **59**, 1853–1864 (2014).
23. Carr, M.-E. & Kearns, E. J. Production regimes in four Eastern Boundary Current systems. *Deep Sea Res. Part II: Topical Stud. Oceanogr.* **50**, 3199–3221 (2003).
24. Browning, T. J. et al. Nutrient co-limitation at the boundary of an oceanic gyre. *Nature* **551**, 242–246 (2017).
25. Hutchings, L. et al. The Benguela current: an ecosystem of four components. *Prog. Oceanogr.* **83**, 15–32 (2009).
26. Lutjeharms, J., Shillington, F. & Duncombe Rae, C. Observations of extreme upwelling filaments in the Southeast Atlantic Ocean. *Science* **253**, 774–776 (1991).
27. Mohrholz, V. et al. Cross shelf hydrographic and hydrochemical conditions and their short term variability at the northern Benguela during a normal upwelling season. *J. Mar. Syst.* **140**, 92–110 (2014).
28. de Boyer Montégut, C., Madec, G., Fischer, A. S., Lazar, A. & Iudicone, D. Mixed layer depth over the global ocean: An examination of profile data and a profile-based climatology. *J. Geophys. Res. Oceans* **109**, C12 (2004).
29. Garaba, S. P. & Zielinski, O. Comparison of remote sensing reflectance from above-water and in-water measurements west of Greenland, Labrador Sea, Denmark Strait, and west of Iceland. *Opt. Express* **21**, 15938–15950 (2013).
30. Patey, M. D. et al. Determination of nitrate and phosphate in seawater at nanomolar concentrations. *TrAC Trends Anal. Chem.* **27**, 169–182 (2008).
31. Welschmeyer, N. A. Fluorometric analysis of chlorophyll a in the presence of chlorophyll b and pheopigments. *Limnol. Oceanogr.* **39**, 1985–1992 (1994).

32. Van Heukelem, L. & Thomas, C. S. Computer-assisted high-performance liquid chromatography method development with applications to the isolation and analysis of phytoplankton pigments. *J. Chromatogr. A* **910**, 31–49 (2001).
33. Mackey, M., Mackey, D., Higgins, H. & Wright, S. CHEMTAX-a program for estimating class abundances from chemical markers: application to HPLC measurements of phytoplankton. *Mar. Ecol. Prog. Ser.* **144**, 265–283 (1996).
34. Higgins, H. W., Wright, S. & Schluter, L. Quantitative interpretation of chemotaxonomic pigment data. In *Phytoplankton Pigments: Characterization, Chemotaxonomy and Applications in Oceanography* **15** (eds Llewellyn, S., Roy, S., Egeland, E. S. & Johnsen, G) 257–313 (Cambridge University Press, 2011).
35. Jeffrey, S. W., Wright, S. W., & Zapata, M. Microalgal classes and their signature pigments. In *Phytoplankton Pigments: Characterization, Chemotaxonomy and Applications in Oceanography* **15** (eds Llewellyn, S., Roy, S., Egeland, E. S. & Johnsen, G) 3–77 (Cambridge University Press, 2011)
36. Kramer, S. J. & Siegel, D. A. How can phytoplankton pigments be best used to characterize surface ocean phytoplankton groups for ocean color remote sensing algorithms? *J. Geophys. Res. Oceans* **124**, 7557–7574 (2019).
37. Catlett, D. & Siegel, D. Phytoplankton pigment communities can be modeled using unique relationships with spectral absorption signatures in a dynamic coastal environment. *J. Geophys. Res. Oceans* **123**, 246–264 (2018).
38. Kirk, J. T. Point-source integrating-cavity absorption meter: theoretical principles and numerical modeling. *Appl. Opt.* **36**, 6123–6128 (1997).
39. Röttgers, R. & Doerffer, R. Measurements of optical absorption by chromophoric dissolved organic matter using a point-source integrating-cavity absorption meter. *Limnol. Oceanogr. Methods* **5**, 126–135 (2007).
40. Garaba, S. & Zielinski, O. Methods in reducing surface reflected glint for shipborne above-water remote sensing. *J. Eur. Opt. Soc.-Rapid Publ.* **8**, 13058 (2013).
41. Garaba, S. P., Voß, D., Wollschläger, J. & Zielinski, O. Modern approaches to shipborne ocean color remote sensing. *Appl. Opt.* **54**, 3602–3612 (2015).
42. Gould, R., Arnone, R. & Sydor, M. Absorption, scattering, and remote-sensing reflectance relationships in coastal waters: testing a new inversion algorithm. *J. Coast. Res.* **17**, 328–341 (2001).
43. O'Reilly, J. E. et al. Ocean color chlorophyll algorithms for SeaWiFS. *J. Geophys. Res. Oceans* **103**, 24937–24953 (1998).
44. Hu, C. et al. Dynamic range and sensitivity requirements of satellite ocean color sensors: learning from the past. *Appl. Opt.* **51**, 6045–6062 (2012).
45. Bricaud, A., Morel, A., Babin, M., Allali, K. & Claustre, H. Variations of light absorption by suspended particles with chlorophyll a concentration in oceanic (case 1) waters: analysis and implications for bio-optical models. *J. Geophys. Res. Oceans* **103**, 31033–31044 (1998).
46. Bricaud, A., Babin, M., Morel, A. & Claustre, H. Variability in the chlorophyll-specific absorption coefficients of natural phytoplankton: analysis and parameterization. *J. Geophys. Res. Oceans* **100**, 13321–13332 (1995).
47. Jassby, A. D. & Platt, T. Mathematical formulation of the relationship between photosynthesis and light for phytoplankton. *Limnol. Oceanogr.* **21**, 540–547 (1976).
48. Baty, F. et al. A toolbox for nonlinear regression in R: the package nlstools. *J. Stat. Softw.* **66**, 1–21 (2015).
49. Louw, D. C. et al. Seasonal and interannual phytoplankton dynamics and forcing mechanisms in the Northern Benguela upwelling system. *J. Mar. Syst.* **157**, 124–134 (2016).
50. Bergen, B., Herlemann, D. P. & Jürgens, K. Zonation of bacterioplankton communities along aging upwelled water in the northern Benguela upwelling. *Front. Microbiol.* **6**, 621 (2015).
51. Wasmund, N. et al. Phytoplankton stimulation in frontal regions of Benguela upwelling filaments by internal factors. *Front. Mar. Sci.* **3**, 210 (2016).
52. Behrenfeld, M. J. et al. Controls on tropical Pacific Ocean productivity revealed through nutrient stress diagnostics. *Nature* **442**, 1025–1028 (2006).
53. Bibby, T. S., Nield, J. & Barber, J. Iron deficiency induces the formation of an antenna ring around trimeric photosystem I in cyanobacteria. *Nature* **412**, 743–745 (2001).
54. Raven, J. A., Evans, M. C. & Korb, R. E. The role of trace metals in photosynthetic electron transport in O 2-evolving organisms. *Photosynth. Res.* **60**, 111–150 (1999).
55. Strzepek, R. F. & Harrison, P. J. Photosynthetic architecture differs in coastal and oceanic diatoms. *Nature* **431**, 689–692 (2004).
56. Berera, R. et al. A mechanism of energy dissipation in cyanobacteria. *Biophys. J.* **96**, 2261–2267 (2009).
57. Stegmann, P., Lewis, M., Davis, C. & Cullen, J. Primary production estimates from recordings of solar-stimulated fluorescence in the equatorial Pacific at 150° W. *J. Geophys. Res. Oceans* **97**, 627–638 (1992).
58. Laney, S. R., Letelier, R. M. & Abbott, M. R. Parameterizing the natural fluorescence kinetics of Thalassiosira weissflogii. *Limnol. Oceanogr.* **50**, 1499–1510 (2005).
59. Hu, C., Feng, L. & Lee, Z. Uncertainties of SeaWiFS and MODIS remote sensing reflectance: implications from clear water measurements. *Remote Sens. Environ.* **133**, 168–182 (2013).
60. Feng, L. & Hu, C. Cloud adjacency effects on top-of-atmosphere radiance and ocean color data products: a statistical assessment. *Remote Sens. Environ.* **174**, 301–313 (2016).
61. Werdell, P. J. et al. The plankton, aerosol, cloud, ocean ecosystem mission: Status, science, advances. *Bull. Am. Meteorol. Soc.* **100**, 1775–1794 (2019).

Acknowledgements

We thank the captain, crew and scientists of the RV Meteor M187 cruise. L. Kraft, Z. Wen, and Z. Chen are thanked for assistance at sea. We are grateful to A. Nicolas for her help with nutrient data organization. We thank B. Bogner, A. Mutzberg, K. Nachtigall, and L. Hansen for technical laboratory assistance. J. Balaguer is thanked for valuable discussion. The research cruise was funded by the Deutsche Forschungsgemeinschaft (DFG, Project-GPF 20-1_036 ReSEAt). S.P.G received support from Deutsche Forschungsgemeinschaft (DFG, Project No. 417276871). T.B.R and T.J.B were funded by the European Union (ERC, Ocean Glow, 101041453). Views and opinions expressed are however those of the author(s) only and do not necessarily reflect those of the European Union or the European Research Council. Neither the European Union nor the granting authority can be held responsible for them.

Author contributions

T.J.B. and T.B.R. designed the study. T.B.R., H.L., S.P.G., D.V., N.S., E.P.A., and T.J.B. conducted the fieldwork/sample analysis. T.B.R. conducted the data analysis. C.M.M. and K.O. contributed to data interpretation. T.B.R. and T.J.B. wrote the paper and all authors provided comments.

Funding

Open Access funding enabled and organized by Projekt DEAL.

Competing interests

The authors declare no competing interests.

Additional information

Supplementary information The online version contains supplementary material available at https://doi.org/10.1038/s43247-025-03067-6.

Correspondence and requests for materials should be addressed to Tiera-Brandy Robinson.

Peer review information *Communications Earth & Environment* thanks Greg Silsbe and the other, anonymous, reviewer(s) for their contribution to the peer review of this work. Primary Handling Editors: Michael Stukel and Alice Drinkwater. [A peer review file is available].